Available online at www.sciencedirect.com
SCIENCE DIRECT®
Journal of Solid State Chemistry 177 (2004) 1994–2001
JOURNAL OF SOLID STATE CHEMISTRY
http://elsevier.com/locate/jssc

Phase evolution of lead titanate from its amorphous precursor synthesized by the OPM wet-chemical route

Emerson R. Camargo,[a,*] Elson Longo,[a] Edson R. Leite,[a] and Valmor R. Mastelaro[b]

[a] *LIEC-Departamento de Química, UFSCar. Universidade Federal de São Carlos, Rod. Washington Luiz km 235, São Carlos SP, Caixa Postal 676, 13565-905 São Carlos, SP, Brazil*

[b] *IFSC-Instituto de Física de São Carlos USP, São Carlos SP, CP 369, 13560-970, Brazil*

Received 19 September 2003; received in revised form 25 December 2003; accepted 23 January 2004

Abstract

Lead titanate was synthesized by the OPM wet-chemical route by the dissolution of Ti metal in H_2O_2 followed by the addition of Pb^{2+} at high pH, resulting in a reactive and amorphous precipitate with (Pb:Ti = 1:1) mole ratio, which was heat treated between 400°C and 700°C. The amorphous precipitate was characterized by DSC, and all of the powders were characterized by X-ray diffraction, Raman and XAS (EXAFS and XANES) spectroscopy at the Ti *K* edge. A metastable, stoichiometric and cubic pyrochlore phase ($Pb_2Ti_2O_6$, *Fd3m*) was identified by XRD and Raman spectroscopy up to approx. 450°C. Only tetragonal $PbTiO_3$ was identified at higher temperatures. XAS spectra showed that the local structure around the absorbing Ti atom of the intermediate pyrochlore phase is similar to that observed in the amorphous precursor. This fact indicates that the metastable intermediate pyrochlore ($Pb_2Ti_2O_6$) is kinetically favored to be formed because of its similarity to the amorphous precipitate, instead of the slightly different and thermodynamically favored tetragonal ($PbTiO_3$, *P4/mmm*) perovskite structure that is only formed at higher temperatures, after the crystallization of the metastable intermediate pyrochlore.

Keywords: Lead titanate; Wet-chemical synthesis; OPM route; Metastable intermediate

1. Introduction

Alternative synthetic routes have been developed for the synthesis of advanced materials. Most of these materials present some unique properties, which is a result of the nanometric size of the particles obtained using some special processing conditions. [1] One of us developed recently a new synthetic route called "the oxidant peroxo method (OPM)" used to prepare several lead perovskites (e.g., $PbTiO_3$ and some compositions of PZT) at relatively low temperature with a sharp particle size distribution of nanoparticles [1–5] and a high final yield of approx. 100% [2]. This method can be well described as a molecular level oxy-reduction reaction between lead ions and some metal-peroxo complexes, at high pH, that forms an amorphous, chemically homogeneous and reactive intermediate precipitate. This precipitate is completely free from carbon, halides or other chemical impurities, what is a remarkable characteristic of the OPM route when compared to others conventional wet-chemical methods of synthesis, such as sol–gel, [6,7] hydrolysis of alkoxides, partial oxalate [8] and the polymerizable complex methods (also known as the Pechini method) [9,10]. Moreover, the OPM technique uses water as solvent and a relatively simple experimental apparatus, without the necessity of dry atmosphere or toxic compounds.

Although the inherent advantage of the OPM route, the nature of the amorphous precursor and the crystallization mechanism is still unknown. Considering that most of the final properties of a material synthesized by wet-chemical methods result from the properties of its initial precursor, we were interested in to describe the local structure of the amorphous precursor obtained by the OPM route when applied for the synthesis of lead-based perovskites. In this context, X-ray absorption fine structure (XAS) spectroscopy is a powerful characterization tool to probe the local structure around a specific element. [11] In this paper, we describe the structure at

*Corresponding author. Fax: +55-16-260-8350.
E-mail address: camargo@liec.ufscar.br (E.R. Camargo).

0022-4596/$ - see front matter © 2004 Elsevier Inc. All rights reserved.
doi:10.1016/j.jssc.2004.01.020

the short range order around Ti atoms in the amorphous precipitate (with mole ratio of Pb:Ti = 1:1) and their heat-treated powders by the use of XAS technique at the titanium *K*-edge. Moreover, additional structural and chemical information were also obtained by means of Fourier transform Raman spectroscopy, differential scanning calorimetry (DSC) and X-ray powder diffractometry (XRD).

2. Experimental section

2.1. Synthesis

Amorphous precipitate with mole ratio (Pb:Ti = 1:1) was synthesized as described by Camargo and Kakihana [2] through the dissolution of 0.250 g of titanium metal powder (98% Wako Pure Chemical Ind Ltd, Japan) in an aqueous solution of 80 mL of H_2O_2 (30% Mallinckrodt, Brazil) and 20 mL of ammonia aqueous solution (30%, Mallinckrodt, Brazil). After approx. 5 h, a yellow transparent solution of peroxytitanate complexes was obtained, and a second aqueous solution of 1.729 g of $Pb(NO_3)_2$ (99.99%, Aldrich, USA) was slowly dropped into the peroxytitanate solution, forming an orange precipitate that was filtered and washed with diluted ammonia solution to eliminate all of the nitrate ions. The washed precipitate was dried at 50°C for 5 h, ground and calcined at several temperatures between 200°C and 700°C (from 5 to 60 min).

2.2. DSC, Raman and XRD characterization

A small amount of the ground and dry amorphous precipitate (10.4 mg) was characterized by differential scanning calorimetry (DSC 404C controlled by TASC 424/3A, Netzsch, Germany) between 25°C and 1200°C using a platinum crucible. It was used a constant heating/cooling rate of 10°C/min and a flux of 0.50 cm^3/min of air. All of the powders (amorphous and heat-treated) were characterized at room temperature by Fourier transform Raman spectroscopy (FT Raman-Bruker RFS 100/S) using the 1063 nm line of a YAG laser, and by XRD using the Cu $K\alpha$ radiation (Rigaku D/MAX 200, with a rotary anode operating at 150 kV and 40 mA) in the 2θ range from 10 to 80° with step scan of 0.02°.

2.3. XAS characterization

The titanium *K*-edge (4966 eV) X-ray absorption spectra were collected at the Laboratório Nacional de Luz Síncrotrom (LNLS, Campinas SP, Brazil) facility using the D04B-XAS1 beam line [12]. The LNLS storage ring was operated at 1.36 GeV and 100–160 mA. XAS data of the amorphous and heat-treated powders were collected in the transmission mode at room temperature using a Si(111) channel-cut monochromator. Ionization chambers were used to detect the incident and transmitted flux. X-ray absorption near edge structure (XANES) at the Ti *K*-edge were recorded for each sample between 4910 and 5200 eV using energy steps of 0.5 eV. Extended X-ray absorption fine structure (EXAFS) measurements at the Ti *K*-edge (using steps of 2 eV) were carried out for each sample between 4840 and 5900 eV. To provide good energy reproducibility during the XANES data collection, the energy calibration of the monochromator was checked after each spectrum using a Ti metal foil.

The EXAFS analysis was carried out by using the software suite written by Michalowicz [13] according to the recommended procedures described by the International Workshop on Standards and Criteria in XAS [14]. After atomic absorption removal and normalization, the $k^3\chi(k)$ weighted EXAFS signal was Fourier transformed to *R* distance space in the 2.0–11.0 $Å^{-1}$ *k* range. Each spectrum was Fourier transformed using a Kaiser apodisation window with $\tau = 2.5$. For comparison purpose between different samples, all XANES spectra obtained at the Ti *K*-edge were background removed and normalized using as unity the first EXAFS oscillation.

3. Results and discussions

Studying the synthesis of lead titanate ($PbTiO_3$, thereafter denoted PT) by means of the Pechini method, Leite et al. [15] suggested, based on XRD and DSC analysis, that a cubic-like intermediate phase crystallizes directly from the amorphous precursor, and that the PT tetragonal perovskite structure (referred to as tetragonal) is formed from this cubic-like phase at 444°C when the temperature is raised. However, it is possible that the energy released from the burning of the organic matrix, as observed by presence of exothermic peaks in the DSC curve, interfered in the crystallization process. On the other hand, Fu et al. [16] reported that nanocrystalline PT ($\sim$7 nm) synthesized by sol–gel route is orthorhombic at room temperature, changing to tetragonal phase at 166°C. Although both of the studies show the presence of different structures, they agree with the presence of a crystalline phase other than the tetragonal phase in nanocrystals of PT at low temperature.

Fig. 1 shows DSC curves between 100°C and 700°C of the amorphous precipitate during the (a) heating and (b) cooling steps. The crystalline state of the material during the DSC experiment is indicated on the top of the curves. The peak centered at 490°C in the heating curve (Fig. 1a) can be assigned to the phase transition from the tetragonal to the high-temperature PT cubic paraelectric perovskite phase (referred to as cubic). The broad

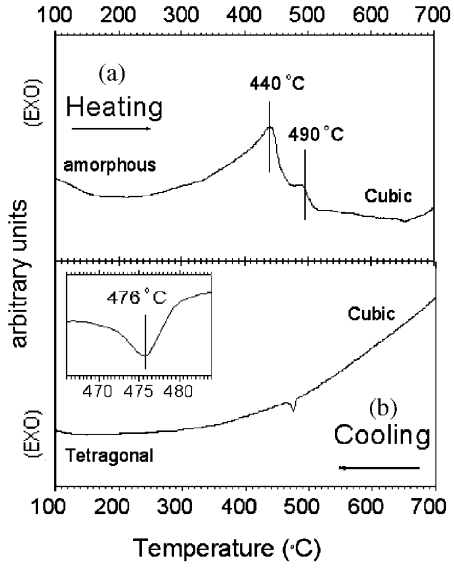

Fig. 1. DSC curves of the amorphous precipitate obtained during (a) the heating step, and (b) during the cooling process. The inset in (b) shows the endothermic peak of the phase transition from the cubic PT to the tetragonal PT. Observe that there is not any other phase transition at temperatures below 475°C.

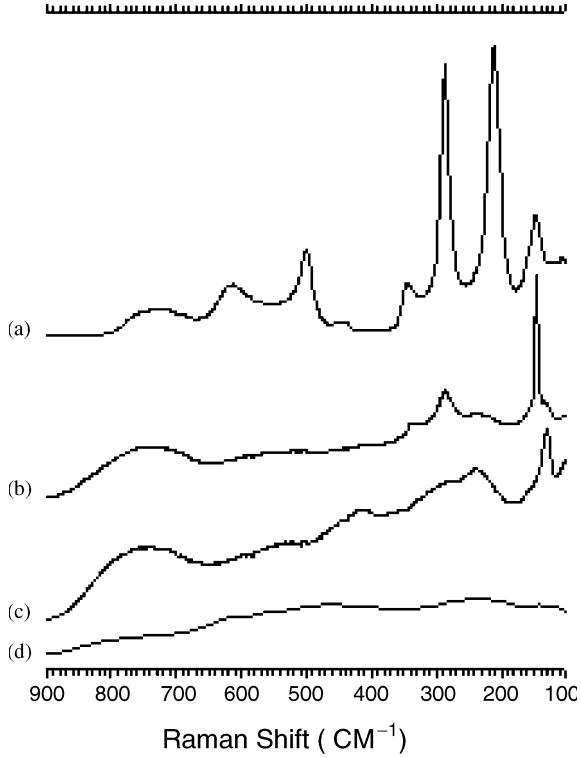

Fig. 2. FT-Raman spectra of (a) PT700, (b) PT450–40, (c) PT 450–15, and (d) of the amorphous precursor.

exothermic peak between 200°C and 470°C with maximum at 440°C can be assigned to the crystallization process from the amorphous precipitate. The small endothermic peak at 476°C in the cooling curve (Fig. 1b) can be assigned to the transition from the cubic to the tetragonal phase.

It is well known that Raman spectroscopy is a suitable structural analytical technique for identification of crystalline phases in nanocrystals when XRD has not enough resolution [17]. Fig. 2 shows Raman spectra collected at room temperature of the amorphous precipitate and of three heat-treated samples. The spectrum (a) of the powder calcined at 700°C for 1 h (referred to as PT700) shows the typical spectra of the tetragonal phase [2]. Spectra (b) and (c), obtained from the powders calcined at 450°C for 40 min (PT450–40) and for 15 min (PT450–15) respectively, show completely different spectra that cannot be assigned neither as tetragonal nor as cubic PT phases. Yao et al. [18] reported the formation of a metastable stoichiometric cubic pyrochlore ($Pb_2Ti_2O_6$) phase at low temperature (identified only by XRD) prior to the crystallization of the tetragonal PT phase during the synthesis of a glass-ceramic materials by a sol–gel route. Moreover, they reported the presence of a sharp exothermic peak at 450°C in some DSC curves, assigned as the crystallization of the tetragonal phase (essentially the same temperature observed in the heating curve of the Fig. 1a). The process described by Yao et al. [18] follows Eq. (1):

$$Pb_2Ti_2O_6 \rightarrow 2PbTiO_3. \quad (1)$$

Although similar spectra to curves (b) and (c) of Fig. 2 were already published [16,19,20], there is not a consensus regarding the structure of the lead titanate formed at low temperature. However, the general shape of the spectrum of Fig. 2b is similar to that observed for the pyrochlore lead pyroniobate ($Pb_2Nb_2O_7$), with main peaks at 145, 231, 285, 334, and 741 cm^{-1}, [20–22] indicating that some correspondence between these two structures ($Pb_2Nb_2O_7$ and the stoichiometric $Pb_2Ti_2O_6$) can be considered. [20] The spectrum of Fig. 2d shows the amorphous nature of the precipitate. It is evident that the presence of three different Raman spectra in Fig. 2 represents three different structural organization of the material, which can be attributed to the crystallization of the stoichiometric cubic pyrochlore structure (Figs. 2b and c) from the amorphous precipitate (Fig. 2d), followed by a phase transition to the tetragonal PT phase (Fig. 2a) at approx. 440°C. This sequence agrees with the previously reported results of the synthesis of lead titanate by wet-chemical methods [15,18–20].

The XRD pattern (a) shown in Fig. 3 was obtained from the powder PT700 (for the sake of clarity, the highest peak (101) was cut at 3% of its height). All of the diffracted peaks were identified as the single tetragonal PT phase, in agreement with the Raman spectrum of Fig. 2a and DSC analysis in Fig. 1. In spite the fact that tetragonal PT could be identified in pattern (b) of the powder calcined at 500°C for 30 min (PT500–30), it is

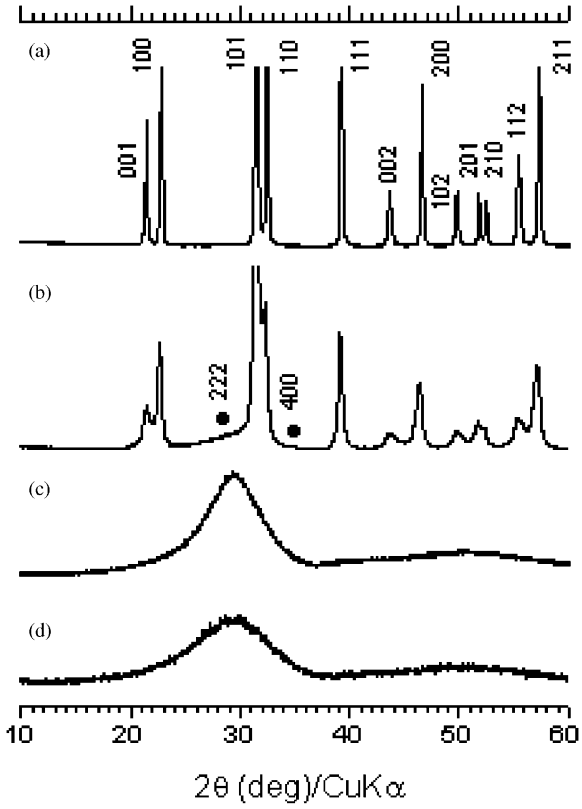

Fig. 3. XRD patterns of (a) PT700, (b) PT500–30, (c) PT 450–15, and (d) of the amorphous precursor.

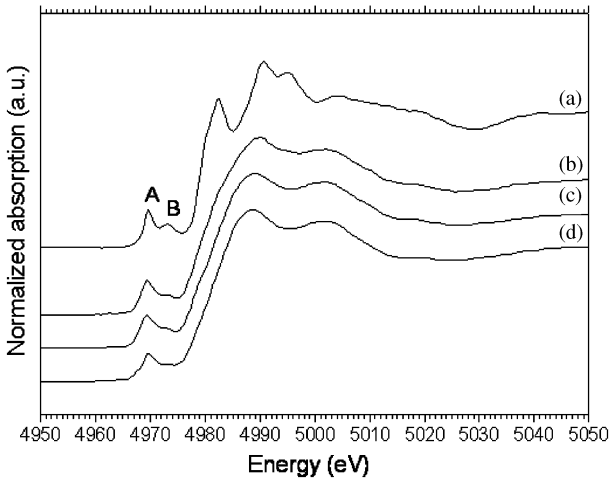

Fig. 4. Titanium *K*-edge XANES spectra of (a) PT700, (b) PT450–40 min, (c) PT450–15, and (d) amorphous precipitate sample.

possible to observe small and broad peaks at 29° and 35° (marked with full circles) indicating that a secondary phase is present. Specifically, the peak at approximately 29° reproduces the same broad peak observed in the XRD patterns (c) and (d) regarding the powder PT450–15 and the amorphous precipitate, respectively. If the stoichiometric cubic pyrochlore $Pb_2Ti_2O_6$ phase is considered as the secondary phase in Fig. 3b, one can assign, based on the Raman evidences of Fig. 2, that these two peaks are the (222) (100%, centered at 29.55°) and the (400) (55%, at 34.33°) diffraction planes of the $Pb_2Ti_2O_6$ pyrochlore phase (PDF card number 26–0142). Therefore, the precipitate seems to crystallize first in the stoichiometric cubic pyrochlore $Pb_2Ti_2O_6$ phase, instead of the thermodynamically expected tetragonal PT.

According to the literature, XANES spectra of transition metal oxides are strongly dependent on the symmetry of the metal site, and titanium (and other transition metals as well) possess unoccupied electron states of *d* character. These states are inaccessible to the dipole excitation of a *s* electron, and the displacement of the transition metal from its centrosymmetric site drives the mixing of *p* character of the transition metal atom. Therefore, the presence of large peaks in a XANES spectrum (e.g., 4965–4975 eV in the titanium case) before the main rise in the spectrum is the signature of a large displacement of the transition atom from its centrosymmetric site [23].

The XANES spectrum obtained at Ti *K*-edge for PT700 shown in Fig. 4a is characteristic of the PT tetragonal phase [23], in agreement with the XRD and Raman results previously discussed (Fig. 2 and 3). The XANES spectra of the samples PT450–40, PT450–15, and of the amorphous precipitate sample (curves (b)–(d) in Fig. 4) exhibit identical edge structure, indicating the same local symmetry for titanium atoms in these three samples. However, these three spectra present a different pre- and post-edge structure when compared with the PT700 tetragonal XANES spectrum (Fig. 4a). The transitions situated at the pre-edge region are less intense, principally in the amorphous precipitate sample (Fig. 4d). The decreasing in the intensity of the transition labeled as *A* in curves (a)–(d) can be attributed to a decreasing in the distortion of the TiO_6 octahedra. According to Veddrinskii [24], the electronic transition assigned as *B* in the XANES spectra does not depend strongly on small displacements of the atoms in the TiO_6 octahedra, but it is mainly affected by structural changes in the vicinity of the absorbing titanium atom.

In the post-edge region of the XANES spectra of Fig. 4, it is observed the presence of large transitions in spectra (b)–(d) in comparison with spectrum (a) of PT tetragonal, where sharp transitions are easily observed. The post-edge transitions in the XANES spectra are mainly due to contributions from multiple scattering effects caused by atoms located in the vicinity of the X-ray absorbing atom, and are used to probe the medium range order around the absorber atom. The broadening in the transitions observed in the post-edge region of

spectra (b)–(d) can be explained by an existence of relative disorder in the medium range structure around the Ti absorbing atom. If these three XANES spectra are compared to results published in the literature, one can see that the pre-edge features are characteristic of pentacoordinated Ti atoms, however, a mixture of fourfold and sixfold coordination cannot be excluded [25,26]. In fact, the XANES spectra (b)–(d) of Fig. 4 are very similar to the XANES spectra of amorphous precursors of $Pb(Zr,Ti)O_3$ ceramics studied by Malic et al. [27]. According to their work, Ti atoms in samples presenting different Zr to Ti ratio are coordinated by five oxygen atoms. Two local symmetry are possible for the Ti pentacoordinating site, the centrosymmetric D_{3h} trigonal bipyramid, and the C_{4v} pyramid with the Ti atom positioned at long of the C_4 axis. [28] Since the centrosymmetric symmetry is not compatible with the XANES spectra, the most probable structure is the C_{4v}. Indeed, to say that titanium atoms are pentacoordinated means, at a first approximation, that the sixth oxygen of the octahedra is located sufficiently far from the titanium atom, which allow us to consider it not coordinated to the titanium, resulting in a highly distorted octahedra.

Fig. 5 presents the EXAFS spectra of PT700, PT450–40, PT450–15 samples, as well the EXAFS spectrum of the amorphous precipitate powder, whilst Fig. 6 illustrates the Fourier transform moduli (FT) of these EXAFS spectra. A qualitative analysis of the EXAFS spectra and of their respective FT curves leads to the same conclusion obtained previously from the analysis of the XANES spectra, i.e., the EXAFS and the FT curves of the PT450–40, PT450–15 and of the amorphous precipitate look very similar, but they differ essentially from those of the PT700. This difference is better noted at high values of k (Fig. 5), where the presence of the EXAFS oscillations are not observed in

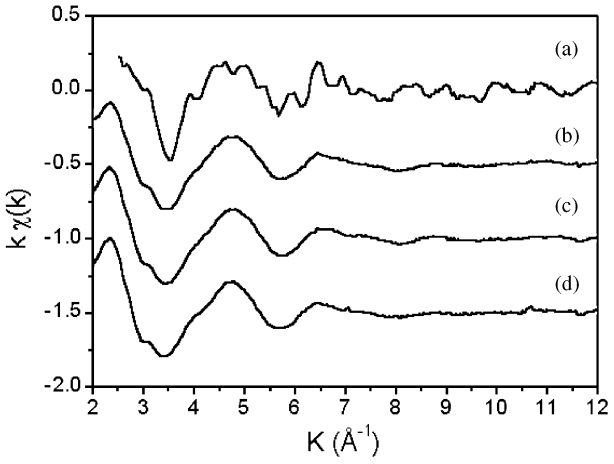

Fig. 5. EXAFS spectra of (a) PT700, (b) PT450–40 min, (c) PT450–15, and (d) amorphous precipitate sample.

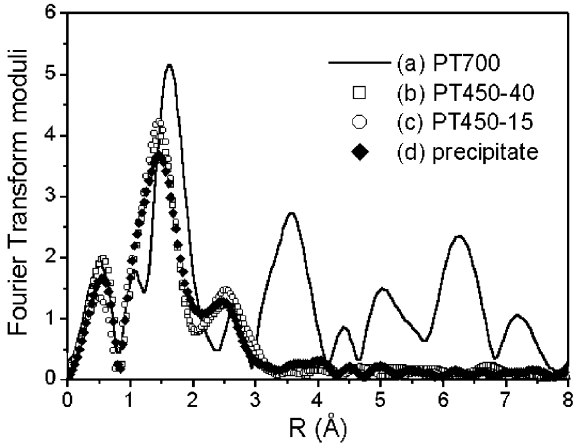

Fig. 6. EXAFS spectra (k-weighted) and corresponding Fourier transforms moduli for: (a) PT700, (b) PT450–40 min, (c) PT450–15, and (d) of the amorphous precipitate sample.

curves (b)–(d), indicating the existence of a high degree of disorder in these samples (confirmed by the absence of structural peaks for distances longer than 3.0 Å in their respective FT curves (b)–(d) in Fig. 6). It should be stressed that other differences are observed between the FT curve of the PT700 and the other FT curves in Fig. 6. The first main difference is the shift toward higher distance of the first Fourier transform peak of curve (a) of PT700 when compared with curves (b)–(d), which is related to the first shell around titanium atoms (Ti–O bonds). An increase in the Ti–O mean bond length is thus expected for the PT tetragonal (PT700) sample. A second significant difference is the increasing in the amplitude of this FT peak of curve (a).

As expected, all of the results (DSC, XRD, Raman and XAS) regarding the well-crystallized PT700 sample confirm that the PT tetragonal phase is formed. However, the most interesting result is obtained when the XAS spectra (EXAFS and XANES) of samples PT450–40 and PT450–15 are compared to their respective XRD and Raman curves and to PT700 results. It is clearly demonstrated by DSC, Raman, XRD and XAS that the crystalline phase obtained after the heat treatment up to 450°C cannot be assigned as the PT tetragonal, but the probable structure seems to be the stoichiometric cubic pyrochlore $Pb_2Ti_2O_6$ with distorted octahedra Ti sites. Comparing the XAS spectra of PT450–40 and PT450–15 samples to the spectrum of the amorphous precursor, one can infer that the local structure around the titanium is essentially the same. Therefore, it is reasonable to conclude that the local order of the amorphous precipitate drives the crystallization into the most favorable structure, that is the $Pb_2Ti_2O_6$. In other words, the structure that posses a similar local organization to the amorphous precursor is preferentially crystallized.

3.1. Quantitative analysis of EXAFS spectra

To obtain a quantitative result from the EXAFS, the spectrum of the crystallized PT tetragonal compound (PT700) was firstly fitted. To do that, the contribution of the first coordination shell of the FT (presented in Fig. 6) was extracted by a back Fourier transform in R space in a range between 0.8 and 2.4 Å, and then fitted using theoretical phase and amplitude functions. To model the Ti–O pair, theoretical amplitude and phase functions were calculated using the FEFF 8.2 program [29]. In all of the fits, the number of free parameters was kept smaller than the number of independent points (defined as $N_{ind} = 2\Delta R\,\Delta k/\pi$ where ΔR is the width of the R-space filter windows, and Δk is the actual interval of the fit in the K space) [14]. The Ti–O oxygen first shell for the crystalline tetragonal $PbTiO_3$ compound was fitted using the three shells model according to the XRD data [30] (e.g., the irregular octahedral Ti site with three different Ti–O bonds length). During the fitting procedure, the coordination number (N) was fixed and the interatomic distance (R) and the Debye–Waller factor (σ) were allowed to vary. A single value of σ was applied for all of the three types of Ti–O bound considered, reducing the number of free parameters during the fitting. Table 1 presents the fitting results and Fig. 7 shows the comparison between the filtered experimental EXAFS spectra of PT700 and the theoretical curve for the crystalline tetragonal $PbTiO_3$. As can be seen in this table, the fitting of the EXAFS spectra agrees with the data found by Glazer [30] using the XRD technique, what validates the procedure used.

Before doing the analysis of the other three samples (PT450–40, PT450–15, and amorphous precipitate) the distance resolution (Δr) that can be achieved during the fitting of these EXAFS spectra was determined as a function of the useful Δk range of the filtered EXAFS spectra. The resolution of the features in EXAFS is limited by the finite range of the data [31], and is determined by the useful Δk range of the filtered EXAFS spectra ($\Delta r = \pi/2\Delta k$). Since the useful Δk range is about 9.0 Å (from 2.5 to 11.5 Å, see Fig. 7 and 8) Δr-values under 0.17 Å cannot be unambiguously resolved. According to the work of Malic et al. [26] titanium atoms in an amorphous lead titanium gel, which was obtained from the hydrolysis of an alkoxide-derived heterometallic complexes, are coordinated by 5 oxygen atoms distributed in two sets of distances (around 1.79 and 1.94 Å). Despite the fact that the difference between these two distances is lower than the resolution determined from the useful Δk range, these two shells model as well the one shell model, were tested for the EXAFS spectra of PT450–40, PT450–15, and for the spectrum of the amorphous precipitate. The results obtained for the fittings of these two models were the same, indicating that the best fitting was achieved when it was assumed that the first shell is formed by 5 oxygens located at 1.94 Å around the titanium atoms (see Table 1). However, this result should be carefully understood. As already discussed, the calculated distance between the oxygens and the titanium atom is affected

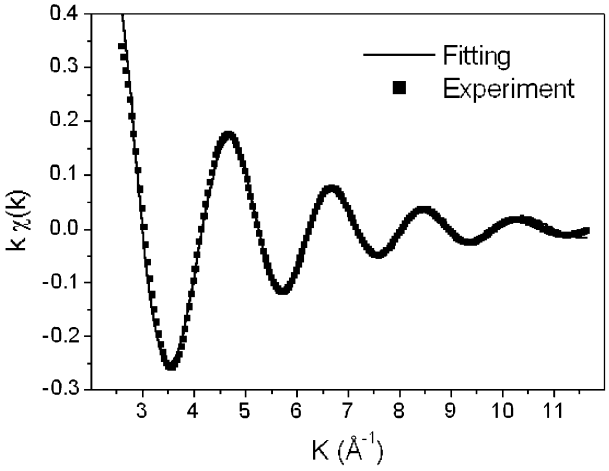

Fig. 7. Fitting and back Fourier filtered signal of the Ti–O first shell for the $PbTiO_3$ tetragonal (PT700) sample using a three-shell model.

Table 1
Fitting results obtained by FEFF 8.2 suit for the tetragonal perovskite sample PT700, and for PT450–40, PT450–15 and for the amorphous precipitate

Sample	N_1	R_1 (Å)	σ_1	N_2	R_2 (Å)	σ_2	N_3	R_3 (Å)	σ_3
Tetragonal $PbTiO_3$ by XRD [30]	4.0	1.98		1.0	1.76		1.0	2.40	
PT 700	4.0	1.99 (±0.01)	0.07 (±0.01)	1.0	1.79 (±0.03)	0.07 (±0.01)	1.0	2.41 (±0.03)	0.07 (±0.01)
PT 450-40	5.0	1.93 (±0.01)	0.102 (±0.005)						
PT 450-15	5.0	1. 93 (±0.01)	0.115 (±0.005)						
Amorphous Precipitate	5.0	1.94 (±0.01)	0.125 (±0.005)						

The results obtained by Glazer et al. [30] are also included. In the table, "N" is related to the number of coordinating oxygens around the Ti atom, "R" is the distance between the oxygen and the Ti atom, and "σ"is the Debye–Waller factor.

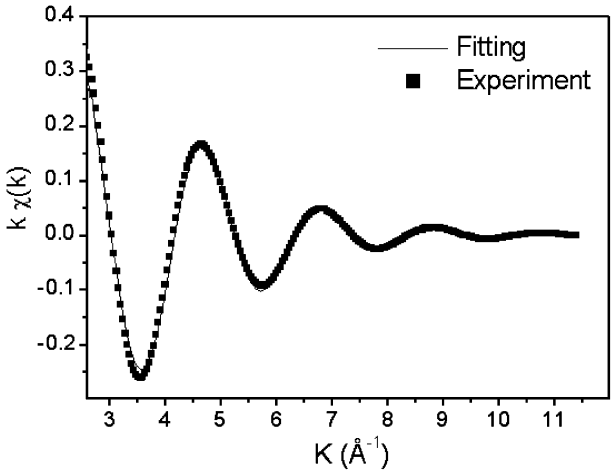

Fig. 8. Fitting and back Fourier filtered signal of the Ti–O first shell for sample PT450–40 using the one-shell fitting model.

by the useful Δk range used for the fitting. Therefore, oxygens located at lightly different distances from the titanium are indistinguishable, resulting that the calculated distance can be an average of distances that differ less than 0.17 Å from each other. The fitting results are presented in Table 1, and Fig. 8 shows the comparison between the filtered experimental EXAFS spectrum of the PT450–40 and its theoretical curve, when the one shell-fitting model was used.

3.2. General discussion and considerations

When the fitting results of the PT450–40 (Fig. 8 and Table 1) are interpreted considering the XANES analysis regarding the titanium displacement from its centrosymmetric position, and the fact that Ti atoms are located inside of octahedral sites in the stoichiometric cubic pyrochlore $Pb_2Ti_2O_6$, one can consider that the five coordinating oxygens around the absorbing Ti atom are organized as in the point group C_{4v}. In this spatial configuration, the oxygens are positioned at the five vertices of a square-based pyramid and the titanium atom is located in some point in the C_4-axis. A distorted octahedra can be visualized with a sixth oxygen atom located at a distance higher than 2.4 Å (therefore, outside of the first shell considered in the fitting procedure). This assumption of distorted octahedra agrees with the XRD, Raman and XAS results.

Moreover, the results indicate that the spatial arrangement of the oxygen and titanium elements in the C_{4v} symmetry point group is formed immediately during the precipitation of the amorphous material, that is during the oxy-reduction reaction between Ti-peroxo complexes and the Pb^{2+} ions. The similarity of the EXAFS and XANES spectra between the amorphous precipitate, PT400–15 and PT400–40 indicates that these samples present similar titanium local structures. This observation can explain the reason why the pyrochlore is formed prior to tetragonal perovskite, and why this stoichiometric pyrochlore has been systematically observed during the synthesis of lead titanate by means of several wet-chemical routes. These results indicate that it is easier for the amorphous material to crystallize in the most similar structure ($Pb_2Ti_2O_6$), which is kinetically favored, instead of a slightly different structure (in this case, the tetragonal PT perovskite), although thermodynamically favored.

Evidently, this metastable pyrochlore structure is not obtained by loss of lead, as usually reported, since tetragonal PT with mole ratio of (Ti:Pb = 1:1) is crystallized further, at higher temperature. If the structure is the pyrochlore-lead deficient type, it should be stable even at heat treatment at high temperatures, and thus easily identified by means of XRD or Raman. However, this lead-deficient phase was not identified after the phase transition to the tetragonal PT. Therefore, it is more plausible that this pyrochlore phase is stabilized by the well-known effect on nanosized particles [32], what turns the identification of this intermediate metastable pyrochlore phase quite difficulty to be characterized. It should be observed that only the phase transition from the stoichiometric pyrochlore ($Pb_2Ti_2O_6$) to the tetragonal PT phase could be identified, without any signal of the reverse phase transition. On the other hand, the transition between tetragonal PT and cubic PT phases was easily identified. It means that is possible to bypass this intermediate phase by heat treatment at temperature higher than 450°C, as indicated by the DSC curves. A general equation for the lead titanate system synthesized by wet-chemical routes can be proposed as

$$2[PbTi]_{(amorphous)} \rightarrow Pb_2Ti_2O_{6(pyrochlore)} \rightarrow 2PbTiO_{3(tretragonal)} \leftarrow \rightarrow 2PbTiO_{3(cubic)}, \quad (2)$$

where the first term at left side represents the amorphous precursor, with mole ratio of (Pb:Ti = 1:1), which can be obtained by several wet-chemical methods (e.g. sol–gel, Pechini, OPM, etc). The unidirectional arrows means that the phase transition can occur only in the indicated direction and consequently, the bi-directional arrow means that the phase transition can occurs in both directions.

4. Conclusions

Despite the fact that single phase tetragonal lead titanate ($PbTiO_3$) perovskite can be obtained by the "oxidant peroxo method-OPM" at relatively low temperature, it was observed that an intermediate cubic and stoichiometric pyrochlore ($Pb_2Ti_2O_6$) phase is formed prior to the expected tetragonal $PbTiO_3$, as supported by the XRD and Raman analysis. Moreover,

XAS spectra of the powders calcined at temperatures up to 450°C show that the coordination sites around the titanium atom are essentially the same of the amorphous precipitate, but different from that observed in the tetragonal $PbTiO_3$. This result indicates that the crystallization process from the amorphous precursor favors structures that have their local structure around the titanium atom as that originally found in the amorphous precursor. Considering all of the previously reported studies of the synthesis of $PbTiO_3$ by any wet-chemical routes, it seems that the formation of the pyrochlore $Pb_2Ti_2O_6$ is a general path to obtain pure lead titanate. All of the results lead to same conclusion, which tetragonal $PbTiO_3$ pure tetragonal PT is obtained after the phase transition from the metastable $Pb_2Ti_2O_6$, however the reverse transition from the tetragonal PT to the pyrochlore $Pb_2Ti_2O_6$ does not occur.

Acknowledgments

Acknowledges to LNLS-National Synchrotron Light Laboratory—Brazil, to MCT-Ministry of Science and Technology of Brazil, and to CNPq. This work was supported by FAPESP.

References

[1] A.P. Alivisatos, J. Phys. Chem. 100 (1996) 13226–13239.
[2] E.R. Camargo, M. Kakihana, Chem. Mater. 13 (2001) 1181–1184.
[3] E.R. Camargo, J. Frantti, M. Kakihana, J. Mater. Chem. 11 (2001) 1875–1879.
[4] E.R. Camargo, M. Popa, J. Frantti, M. Kakihana, Chem. Mater. 13 (2001) 3943–3948.
[5] E.R. Camargo, M. Kakihana, J. Am. Ceram. Soc. 85 (2002) 2107–2109.
[6] C.D.E. Lakeman, D.A. Payne, Mater. Chem. Phys. 38 (1994) 305–324.
[7] L.L. Hench, J.K. West, Chem. Rev. 90 (1990) 33–72.
[8] E.R. Camargo, M. Kakihana, E.R. Longo, E.R. Leite, J. Alloys Compounds 314 (2001) 140–146.
[9] M. Kakihana, J. Sol–Gel Sci. Technol. 6 (1996) 7–55.
[10] E.R. Camargo, E. Longo, E.R. Leite, J. Sol–Gel Sci. Technol. 17 (2000) 111–121.
[11] J.J. Rehr, C.A. Albers, Rev. Mod. Phys. 72 (2000) 621–654.
[12] H.C.N. Tolentino, A.Y. Ramos, M.C.M. Alves, R.A. Barrea, E. Tamura, J.C. Cezar, N.J. Watanabe, J. Synchrotron Rad. 8 (2001) 1040–1046.
[13] A. Michalowicz, J. Phys. IV 7 (1997) 235–236.
[14] S.S. Hasnain, Report on the International Workshops on Standarts and Criteria in XAS, in: X-ray Absorption Fine Structure: Proceedings of the VI International Conference on X-ray Absorption Fine Structures, Ellis Horwood, New York, 1991.
[15] E.R. Leite, E.C. Paris, E. Longo, J.A. Varela, J. Am. Ceram. Soc. 83 (2000) 1539–1541.
[16] D. Fu, S. Hisao, K.S. Suzuki, Phys. Rev. B 62 (2000) 3125–3129.
[17] M. Kakihana, M. Yashima, M. Yoshimura, L. Borjesson, M. Kall, Trends Appl. Spectrosc. 1 (1993) 261–311.
[18] K. Yao, W. Zhu, X. Yao, L. Zhang, Mater. Sci. Eng. B 41 (1996) 322–328.
[19] E.R. Leite, E.C. Paris, E. Longo, F. Lanciotti, E.C.M. Campos, P.S. Pizani, V. Mastelaro, C.A. Paskocimas, J.A. Varela, J. Am. Ceram. Soc. 85 (2002) 2166–2170.
[20] D. Bersani, P.P. Lottici, A. Montenero, S. Pigoni, G. Gnappi, J. Non-Cryst. Solids 193 (1995) 490–493.
[21] A. Jayaraman, G.A. Kourouklis, A.S. Cooper, G.P. Espinosa, J. Phys. Chem. 94 (1990) 1091–1094.
[22] N. Wakiya, J. Shiihara, K. Shinozaki, N. Mizutani, J. Sol. State Chem. 143 (1999) 344–348.
[23] B. Ravel, E.A. Stern, R.I. Vedrinskii, V. Kraizman, Ferroelectrics 206 (1998) 407–430.
[24] R.V. Vedrinskii, V.L. Kraizman, A.A. Novakovich, P.V. Demekhin, S.V. Urazhdin, J. Phys.: Condens. Matter 10 (1998) 9561–9580.
[25] Z. Liu, R.J. Davis, J. Chem. Phys. 98 (1994) 1253–1261.
[26] B. Malic, I. Arcon, M. Kosec, A. Kodre, J. Mater. Res. 12 (1997) 2602–2611.
[27] B. Malic, I. Arcon, A. Kodre, M. Kosec, J. Sol–Gel Sci. Technol. 16 (1999) 135–141.
[28] F.A. Cotton, Chemical Applications of Group Theory, 2nd Edition, Wiley-Interscience, New York, 1971.
[29] A.L. Ankudinov, B. Ravel, J.J. Rehr, S.D. Conradson, Phys. Rev. B 58 (1998) 7565–7576.
[30] A.M. Glazer, S.A. Mabud, Acta Crystallogr. B34 (1978) 1065–1078.
[31] D.C. Koningsberger, R. Prins, X-ray Absorption, Principles, Applications, Techniques of EXAFS, SEXAFS and XANES, Wiley, New York, 1988.
[32] C.C. Chen, A.B. Herhold, C.S. Johnson, A.P. Alivisatos, Science 276 (1997) 398–401.